Comparative Study of the Growth of CNTs on Stainless Steel with and without the External Catalyst

Mazdak Hashempour[a], Antonello Vicenzo[a], Massimiliano Bestetti[a]

[a] Dipartimento di Chimica, Materiali e Ingegneria Chimica "Giulio Natta", Politecnico di Milano, Via L. Mancinelli 7, 20131, Milan, Italy

Multi-walled carbon nanotubes were synthesized on 316 stainless steel substrate by chemical vapor deposition through two different methods: 1- without use of any external catalyst and using ethylene as the carbon precursor and 2- using ferrocene as an external source of catalyst particles, dissolved in toluene, as the carbon precursor. Carbon nanotubes grown by the two methods were characterized by scanning and transmission electron microscopy and X-ray diffraction methods and were compared subsequently to determine certain characteristics of each method. Good coverage and homogeneity was observed in both cases. However, the carbon layer was thicker and denser in externally catalyzed samples. Two different mechanisms, namely, *base* and *tip* modes, were observed for the nanotubes growth, each with particular characteristics stemming from the synthesis methods. Surface nano-features and external catalyst behavior were found to have the dominant role in determining the morphology of carbon filaments in intrinsically and externally catalyzed samples, respectively.

Introduction

Chemical vapour deposition (CVD) is a versatile technique for the growth of carbon nanostructures, which has been widely used for the growth of carbon nanotubes (CNTs), e.g. (1), particularly for its capability in terms of higher control and scalability of the process (2).

Notoriously, the catalyst template effect is a key aspect in the control of the type, nature and the morphology of filamentary carbon, either nanotubes or nanofibers, as proven by a wealth of experimental studies and extensively discussed in the literature, see, e.g., a very recent review (2).

Though the growth mechanism of CNT remains still unclear and the control of the structure of CNT challenging, non-catalytic substrate surfaces can be properly engineered, i.e. decorated with catalyst nanoparticles, using various deposition techniques along with specially designed experimental strategies, to achieve such a high degree of growth control that aligned CNT layers have been produced on different substrates and in a range of operating conditions, e.g. (3,4).

A relatively less popular subject in this area is the direct growth on substrates allowing catalysis of CNT. Direct growth of CNT is a straightforward and promising technique for the fabrication of CNT coated metal substrates for a variety of applications. In particular, an area of great interest is the fabrication of high surface area electrodes for energy storage devices, fuel cells and electroanalysis (5), as well as for application in

environmental remediation processes and generally for industrial electrochemistry, e.g. (6). In this respect, a distinctive advantage of direct growth is expected to be higher adhesion of the CNT layer to the substrate, which implies an attendant improvement of other technological properties of the CNT layer-substrate composite.

However, compared to the case of growth activated by an externally applied catalyst (7–14), the control of the template effect is ostensibly more difficult, depending on the ability to modify the surface morphology at the nanoscale, in order to achieve a uniform distribution of growth centres of suitable size and shape. Not surprisingly, relatively few attempts have been made to direct growth on catalytic substrate, namely on cobalt (15,16), nickel (15,17–20) and stainless steel (21–31). Direct growth of CNT on stainless steel (SS) has been studied in some detail, nonetheless the understanding of the mechanistic processes determining the growth characteristics of nanotubes and nanofibers remains incomplete.

In the present work we address some of the issues stemming from the research scenario roughly sketched in the above lines, assuming as a representative case study the CNT growth on SS substrate either by the direct growth method or the externally catalysed process. As an example of the latter, the pyrolysis of hydrocarbons in the presence of ferrocene, which in spite of its wide and successful application to many substrates (32–34) has rarely been used to grow CNTs on SS (35), is used.

Experimental

Materials and preparation

As the substrate material, AISI 316 SS plates of the size 15×15×1 mm were used for all experiments. As a preliminary step before synthesis of the nanotubes, all samples were cleaned with successive sonication in acetone and distilled water, 10 min each, to remove the organic and inorganic pollutant, respectively. Afterwards, all samples were nitrogen dried and transferred to the CVD reactor.

CNT Synthesis without external catalyst

The synthesis procedure of CNTs on 316 SS without external catalyst has been discussed in details in an earlier work (36) and the same method has been followed here. Just as a brief anamnesis, a horizontal quartz tube passing through an electrical furnace with controlled temperature formed the CVD reactor. The tube possessed two inlet channels, one for a mixture of gases and the other for the liquid precursors. The gas inlet was coupled to a gas flow control system to adjust the flow of nitrogen as the carrier gas, hydrogen as the reducing agent and ethylene as the carbon source. Pristine 316 SS samples, fixed on an alumina stage, were placed into the quartz tube. The tube was first purged with a 100 sccm flow rate of carrier gas, nitrogen in accompany with a 6 sccm of hydrogen to remove the oxide layers and avoid surface oxidation during heating. The reactor was heated up to 760 $^{\circ}$C with a heating rate of 15 $^{\circ}$C/min, the temperature being monitored with a thermocouple. After 10 min holding at 760 $^{\circ}$C for temperature stabilization, a flow rate of 20 sccm of carbon precursor, ethylene (C_2H_4), was fed into the reactor for 20 min, in order to sustain the growth. After the growth step, ethylene flow was stopped and the furnace was cooled down under continuous and unchanged flow of N_2 and H_2. For brevity, the sample grown with this method will be referred to as “directly grown (DG)”, hereafter.

CNT Synthesis with ferrocene external catalyst

In this method, a solution of 1 gr of ferrocene, $Fe(C_5H_5)_2$, in 50 ml of toluene was prepared as the source of catalyst and carbon. This solution was connected to the second inlet channel of the quartz tube and was purged with nitrogen before heating up the furnace, in order to avoid any air entering the reactor. Gas composition in the tube during heat-up and stabilization was the same as the first method; 100 sccm of N_2 and 6 sccm of H_2. The final temperature for stabilization and synthesis was set up to 700 $^{\circ}$C and the reactor was heated up with a heating rate of 15 $^{\circ}$C/min. After the stabilization, the solution was admitted into the tube simply through a gravity effect, from the solution container placed on a higher height compared to the reactor. Five drops of the solution were admitted into the tube for 4 times, each time with a subsequent 5 min waiting time for the solution to be evaporated by approaching the hot zone of the furnace and being carried to the reactor center via carrier gas. Therefore, on the whole, a 20 min synthesis time was allowed, after which, solution injection was given up and the reactor was cooled down under the continuous and constant flow of N_2 and H_2. For brevity, the sample grown with this method will be referred to as "catalytically grown (CG)", hereafter.

Characterization

Phase analysis of the grown carbon layer was performed by X-ray diffraction (XRD) in grazing incidence geometry (1830 PW Philips X-ray generator equipped with a PW 3020 Philips goniometer and a PW 3710 Philips control unit). Atomic Force Microscope (AFM, NT-MDT Solver Pro) operated in contact mode was used to characterize the surface topography of samples. Microstructural characterizations of CNTs were carried out using scanning electron microscope (FEI Philips XL30 FEG ESEM) and transmission electron microscope (Philips CM200 FEG TEM). Samples for TEM analysis were prepared by scraping of the CNT layer by a blade into an ethanol container and ultrasonication for 60 min.

Results and Discussion

Fig.1 shows the SEM micrographs of CNTs grown on 316 SS without (a and b) and with (c and d) external catalyst. As can be seen by comparison of Fig.1a and c, the carbon layer in CG sample (Fig.1c) is denser and thicker than DG sample (Fig.1a). Higher magnification images of samples DG and CG are shown in Fig.1b and d, respectively, according to which, certain characteristics can be recognized for each. Sample DG (Fig.1b) shows a wider range of CNT diameters between 20 to 60 nm, with average size larger than CG (Fig.1d). Moreover, a number of thick filaments with a diameter larger than 70 nm can be observed in DG sample which are carbon nanofibers (CNFs). Another interesting characteristic of sample DG, is the presence of tiny particles on tips of some of the CNTs, as pointed by white arrows (Fig.1b), reinforcing the probability of a tip mode CNT growth. However, since this phenomenon is just seen in a limited fraction of CNTs, other mechanisms should be active to facilitate the growth in other CNTs. These mechanisms will be discussed based on the AFM and TEM studies in the following sections. In contrast to DG sample, CNTs grown on CG samples have a more homogeneous size distribution with diameter between 15 to 40 nm and negligible number of CNFs. Moreover, considerable number of small catalyst particles can be observed on

the outer walls of CNTs throughout the sample, as pointed by white arrows in Fig. 1d. Interestingly, growth of new CNTs from the mentioned catalyst particles on CNT walls is observed, forming "V" shaped forks. Two of these offshoots are indicated by black arrows in Fig. 1d.

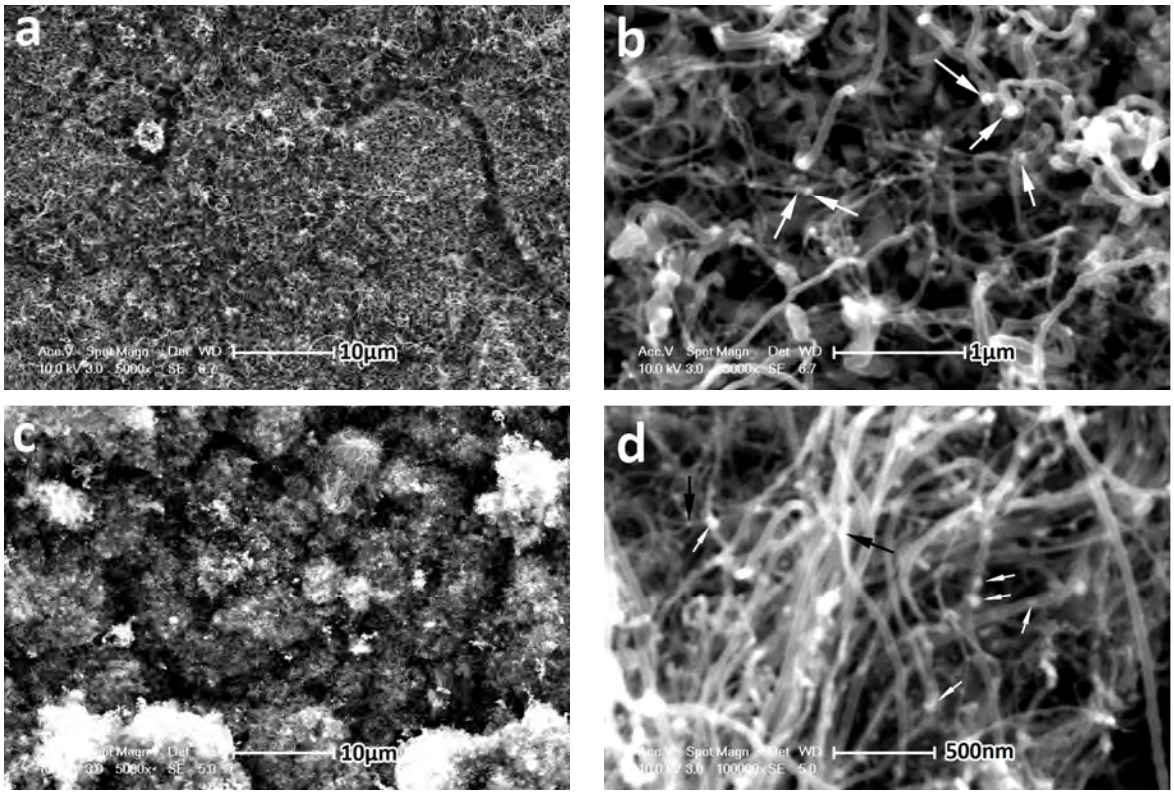

Figure 1. SEM micrographs of samples DG (a and b) and CG (c and d).

Since direct growth of CNTs on SS has been reported to be in direct relation with the surface nano-features of self-catalytic substrate (21,26,29,36,37), a detailed AFM study of the substrate surface was conducted after the primary atmosphere controlled heat up and stabilization steps (referred to as "reducing atmosphere heating" hereafter), before the start of the growth step. Fig.2 shows the results of AFM topography of DG sample and subsequent statistical analysis of the data. High resolution 1µm x 1µm scan of AFM is shown in 3d and 2d modes in Fig.2a and b, respectively. As seen, after the "reducing atmosphere heating" a nano-scale roughness has formed on the substrate surface with an almost homogenous coverage. Preliminary conjectures about the origin of this rarely discussed phenomenon, at least in the context of CNT growth, acknowledge an interplay between surface reconstruction phenomena caused by oxide reduction and adsorption interaction with gas phase components, on the one side, and thermally activated processes, such as phase separation and inhibited or limited recrystallization on the other side, as the underlying motive of the surface restructuring (36). Fig.2c shows the distribution density histogram of the height of surface nano-features based on the data processing of the 3d AFM (Fig.2.a) results. It is seen that these nano-hills possess a narrow height distribution range between 45-55 nm, with 48.5 nm as the statistically calculated average. Roughness analysis results also demonstrated an average roughness of 5.8 nm, implying small fluctuations of the nano-hill heights. Fig.2d shows the normal (Gaussian) distribution

histogram of the lateral size of surface nano-features based on the statistical analysis of the 2d (deflection related signal, DFL mode) AFM (Fig.2.b) results. It is seen that these uniform granular nano-hills possess an average lateral diameter of 55 nm. This is in good agreement with the diameter size of the CNTs. Moreover, the part of nano-features with lateral size over 60 nm could be responsible for the growth of CNFs.

Considering the fact that the "reducing atmosphere heating" process is the same for both samples (except the final temperature that is 60 ^{o}C lower for CG sample), it can be assumed that similar features should have formed also in CG sample, notwithstanding the difference in growth step and carbon precursor. Accordingly, the differences observed in CNTs of the CG sample should be arising primarily from a different growth mechanism. In order to have a more in-depth understanding of the growth mechanism in both samples, XRD and TEM studies were conducted.

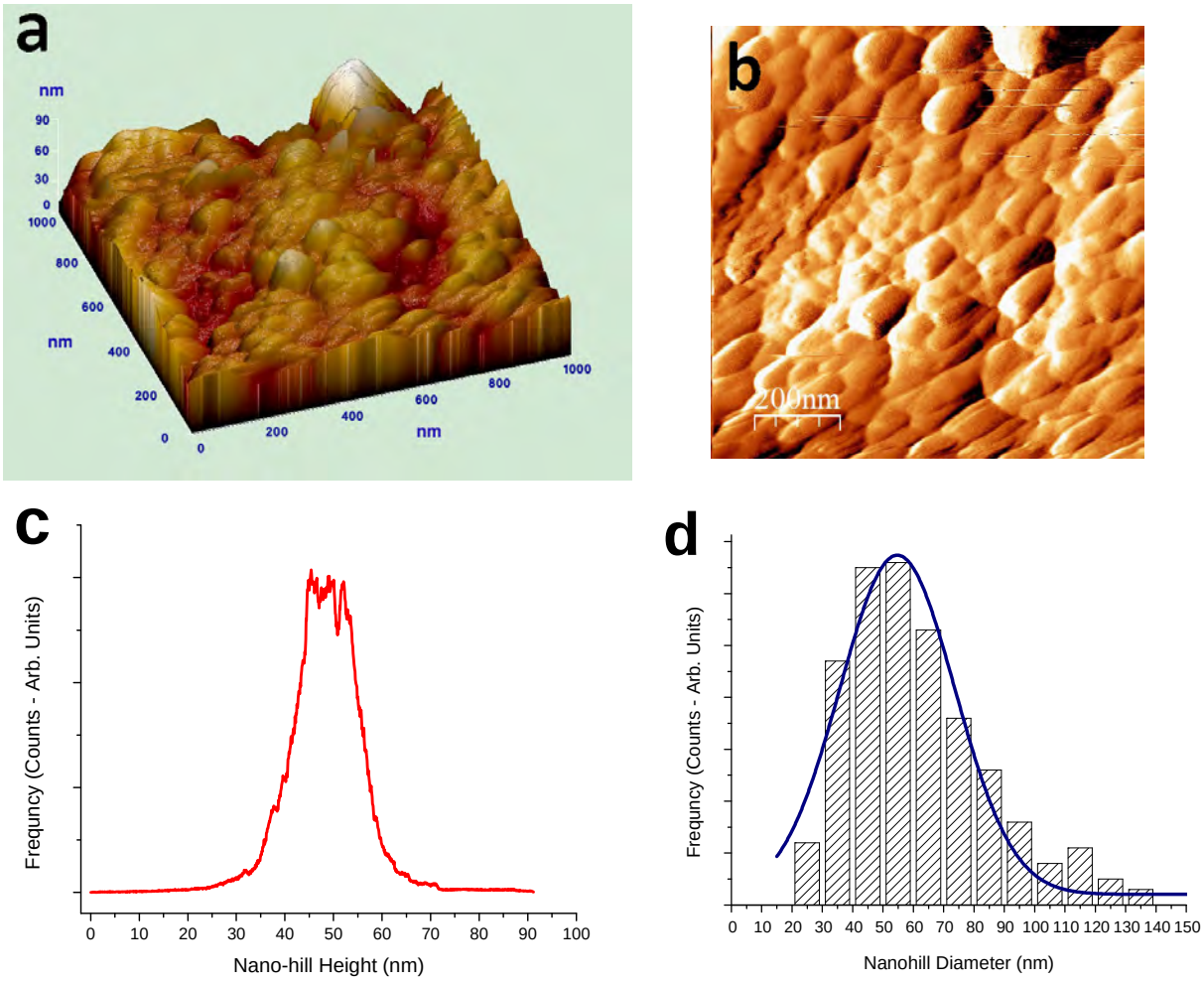

Figure 2. High resolution AFM scan of the sample DG comprising (a) three dimensional topography of the scanned surface, (b) two dimensional deflection (DFL) mode image of the scanned surface, (c) distribution density histogram of the height of surface nano-features and (d) normal (Gaussian) distribution histogram of the lateral size of surface nano-features.

Fig.3 shows the XRD patterns of SS in as-received and as-grown conditions. Characteristic FCC peaks of austenite are detected for bare SS in accompany with weak oxide peaks specifying a thin passive layer on the surface. In case of as-grown samples, characteristic peaks of hexagonal graphite at 2θs 26.1^{o} and 44.6^{o} were observed corresponding to (002) and (101) crystallographic planes, respectively. The first one which is the strongest graphite peak predicts and interplanar spacing of almost 0.34 nm. In the context of CNTs, this spacing corresponds to the distance between the walls of the CNT.

A considerable difference can be realized in the nature of carbide peaks observed in DG and CG samples. While these reflections are weak in DG sample and are most likely stemming from the carburization of SS in contact with ethylene at elevated temperature, carbide peaks of CG sample, clearly Fe_3C, are strong and explicit. Concerning the nature of carbides observed in DG sample and their role in CNT growth, similarities can be found in the literature of dusting corrosion of SS (38–40), in terms of the coexistence of iron and chromium carbides, and partial presence of Cr_2FeO_4.

In contrast to DG sample, carbide peaks in CG sample are straightforward to interpret based on the massive literature discussing the catalytic behavior of the carbide form of iron where initially a pure form of iron is used as the external catalyst (41–43). Similarly, in ferrocene catalyzed growth, immediately after primary evaporation of toluene-ferrocene solution, the vapor enters the hot zone of the furnace and dissociates to iron nanoparticles and hydrocarbons such as phenyl and methyl groups which, in turn, are subject to more dissociation. In any condition, iron nanoparticles, immediately after formation, get

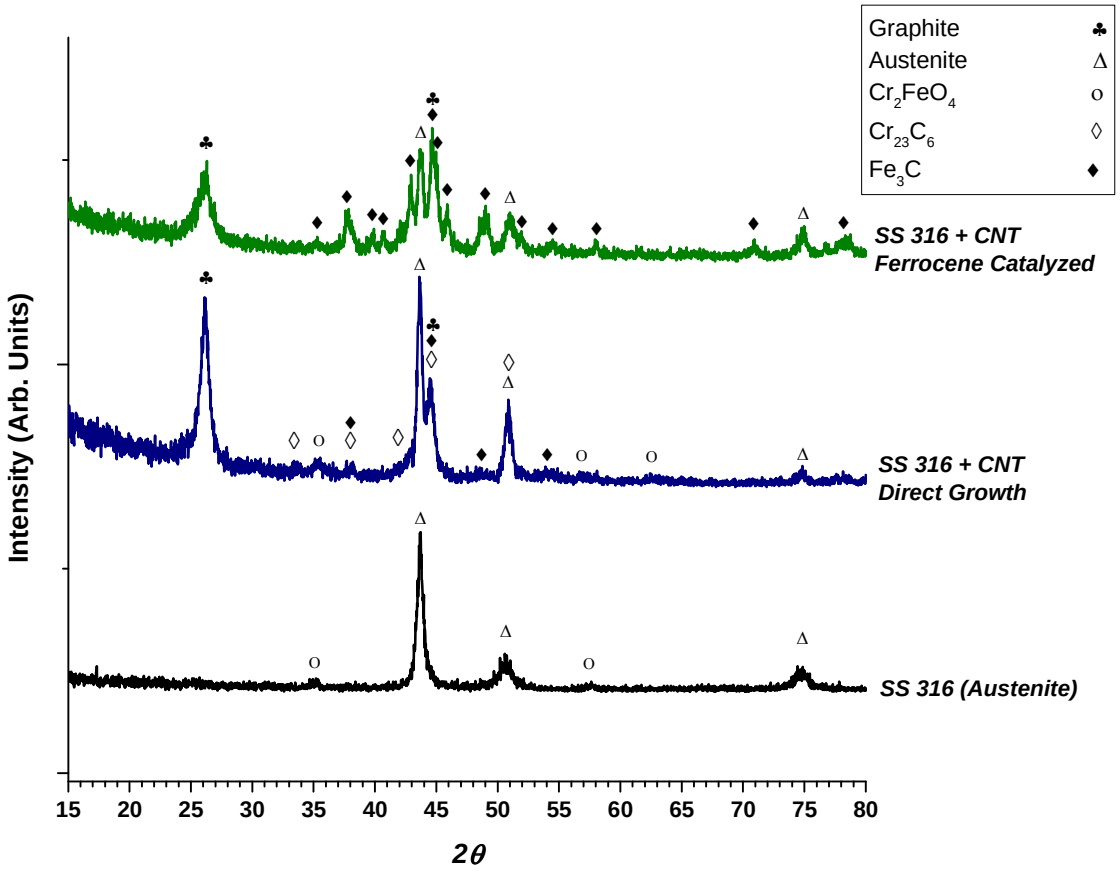

Figure 3. XRD patterns of bare SS, DG and CG samples.

saturated with carbon and serve as nucleation sites of CNTs. Hence, dominant presence of Fe_3C peaks in CG sample should be taken for granted. Evidences of metal dusting are not observed in the XRD patterns of CG sample, though this aspect should be investigated in greater detail.

Fig.4 shows the TEM micrographs of sample DG. Formation of multi-walled carbon nanotubes (MWCNTs) with outer diameter size ranging between 20 to 50 nm and inner diameter in the range of 10 nm is confirmed. Some CNFs were observed in TEM investigations as well, which are not presented here. Catalyst particles, as a key point to understand the growth mechanism, were observed in two different morphologies as shown in Fig.4a and b, corresponding to *base* and *tip* growth modes, respectively. Presence of thin conical shaped nanorods inside the CNT channel, as the one shown in Fig.4a, is believed to represent the base growth mode (44). In case of CNT direct growth on SS, these shoot shaped catalyst have been reported to be originating from the surface nano-features serving as the catalytic sites (21,36). On the other side, presence of relatively large catalyst nanoparticles on CNT tips, as the one shown in Fig.4b, is most

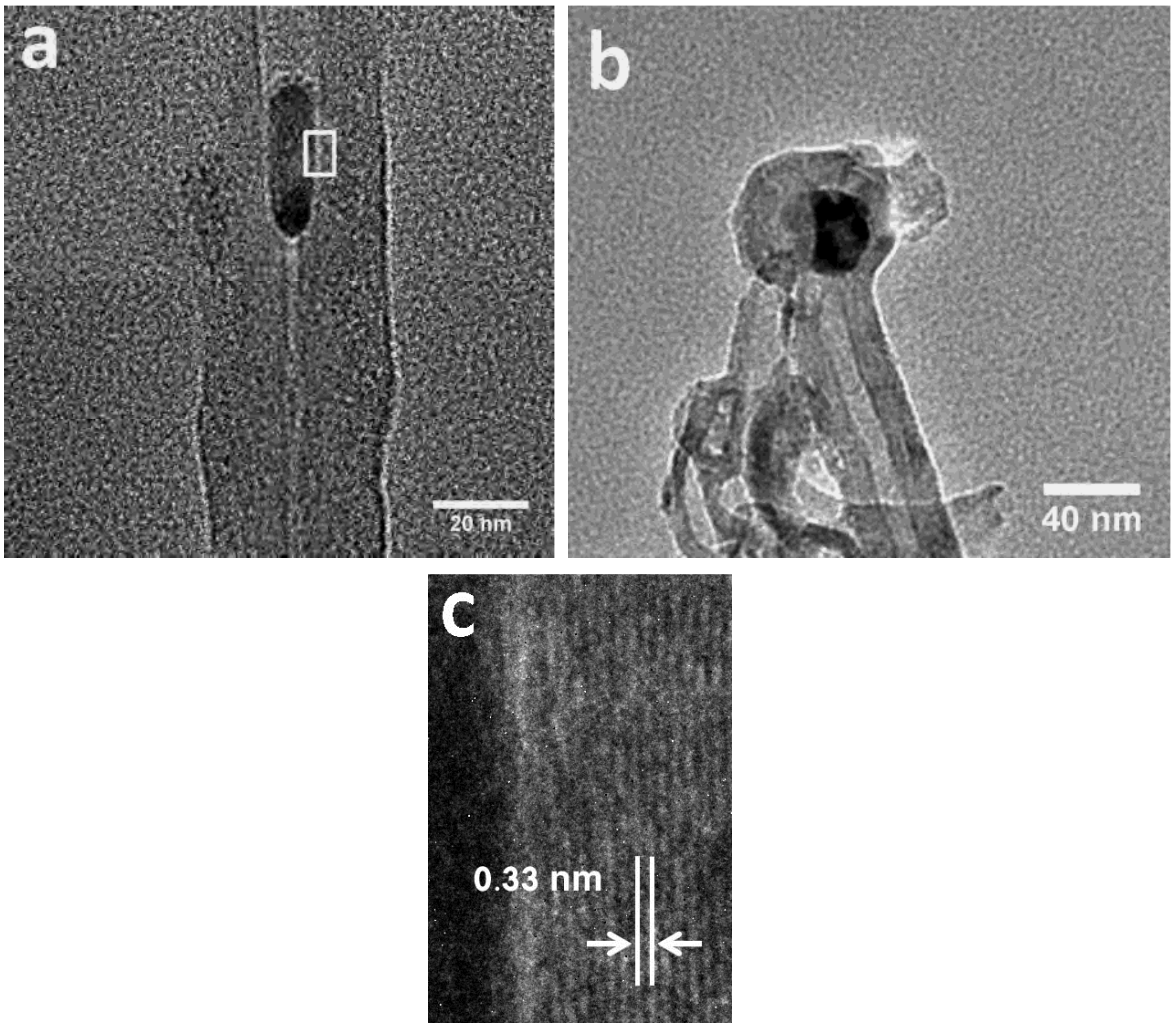

Figure 4. TEM micrographs of sample DG, (a) conical catalyst particle inside the tube, (b) large encapsulated catalyst particle on CNT tip and (c) HRTEM of a walls of MWCNT.

often conceived as a characteristic of tip growth mode (45,46). In case of CNT direct growth on SS, such phenomenon has been attributed to the break-off of surface nano-features due to exposure to high temperature carbonaceous atmosphere (36), or in more specific words, due to “metal dusting” (47,48). Accordingly, presence of the catalyst particles observed in Fig.1b should be caused by the same mechanism. Fig.4c shows a high resolution view of the white rectangle marked area of Fig.4a. An interplanar spacing of 0.33 nm, confirms the calculated value by XRD.

Fig.5 shows the TEM micrographs of sample CG. According to these micrographs, considerable differences can be inferred in the characteristics and the behavior of the catalyst in CG sample. Firstly, multiple nucleation of CNTs on an individual catalyst particle and multidirectional growth of the nucleated CNTs, should be noticed. As Fig.5a shows, a single catalyst particle, encircled by dash lines, is simultaneously nourishing two different CNTs growing in two different directions, 1 and 2, as marked by white

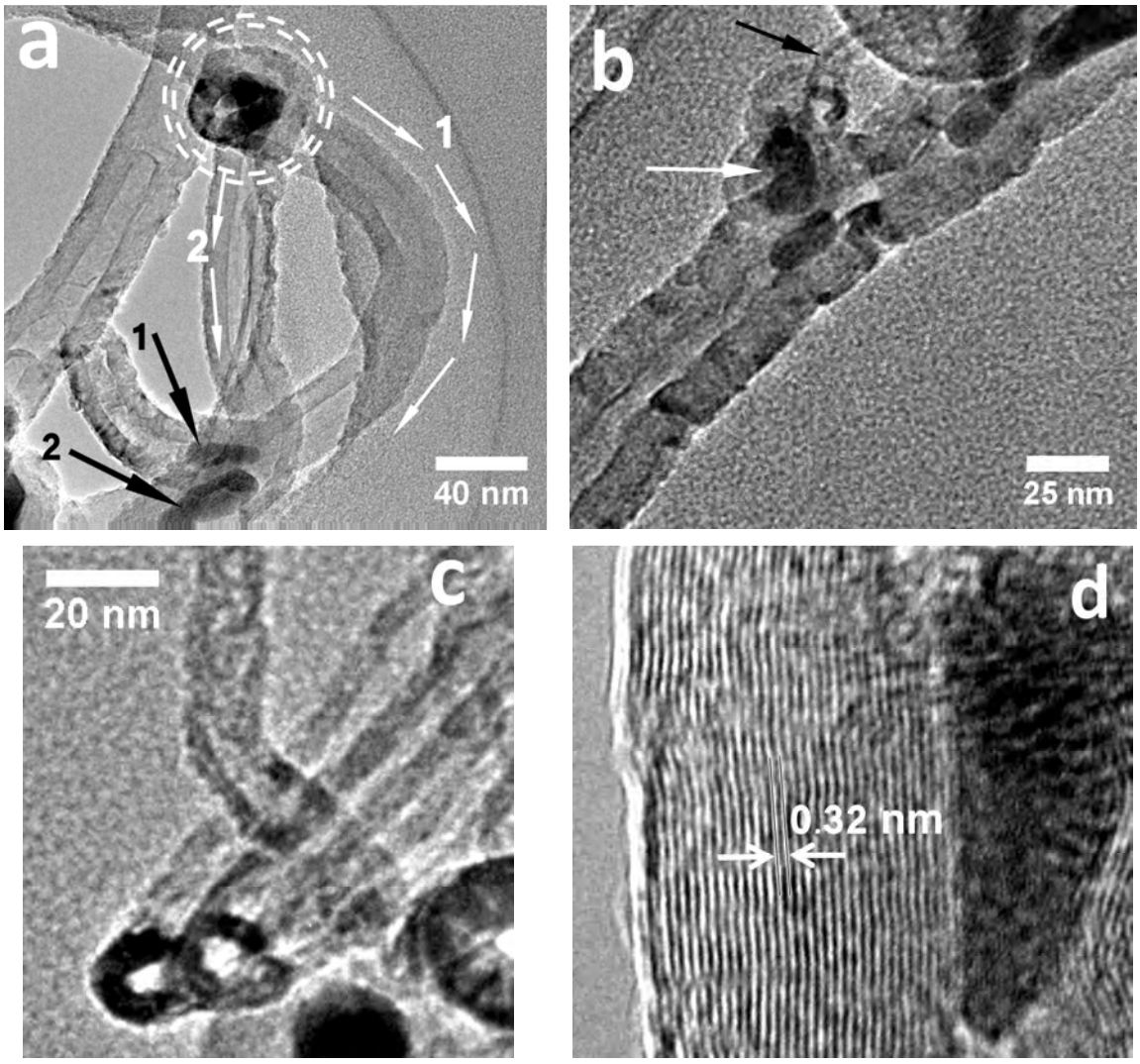

Figure 5. TEM micrographs of sample CG, (a) multiple nucleation and growth of CNTs from a single catalyst particle (twin CNTs), (b) offshoot CNT grown on a catalyst particle deposited on the wall of and elder CNT (parent and child CNTs), (c) open ended CNTs and (d) HRTEM of the walls of a MWCNT.

arrows. It is also seen that in both CNTs, a base growth mode is in progress: in fact, the detached parts of the catalyst particle are injected in the tube channel and move toward the tube tips (particles pointed by black arrows). Since both CNTs are stemming and being fed from the same catalyst, it can be inferred that their nucleation has occurred simultaneously or within a short time lapse and hence, they could be called twin CNTs. Another type of ramification is indicated in Fig.5b, where a newborn CNT (pointed by black arrow) is growing from a recently deposited catalyst particle (pointed by white arrow) on the wall of an already mature CNT. Since in this case both CNTs are not being fed from the same source and one (the newborn or the offshoot) is formed considerably later than the other and relying on its support, they could be called parent and child CNTs. This later type of CNT growth is in agreement with the SEM observations of Fig.1d highlighting the deposition of catalyst particles on CNT walls and subsequent growth of offshoot CNTs on them.

Dissimilar to most of ferrocene catalyzed CNT growth examples in the literature (32,49), tip mode growth is not significant in our study and indeed, instances of presence of the catalyst particles on CNT tips actively supporting the CNT growth could hardly be found in our TEM investigations. This point can be elucidated on the grounds of catalyst-substrate interactions. Since the catalyst used here is originally iron, strong adhesion to the SS substrate, which in turn is basically made of iron, is reasonably assumable. Accordingly, catalyst detachment from the substrate and activation of tip growth mode usually seen in literature for substrates other than SS, is not observed here. This is in agreement with the XRD results of CG sample implying the absence or deficient activation of dusting mechanism. Another feature seen more specifically in CG sample, is the presence of CNTs with open end, as Fig.5c shows two of them. This observation supports the lack, or, weak activation of tip growth mode. The HRTEM micrograph shown in Fig.5d, shows a highly ordered wall arrangement in a MWCNT on CG sample with more than 30 walls. However, this level of order and regularity is not the representative of all MWCNTs grown and observed in this study.

Conclusions

Direct and external catalyst assisted growth of MWCNT on 316 SS were studied via thermal CVD processing. Both methods showed success in formation of homogenous MWCNT layers with good adhesion to SS. Systematic characterization of the CNTs and catalyst particles in the two methods showed that:

1- Growth of CNTs on SS without external catalyst is highly dependent on the surface nano-features. Nano-hills with lateral diameter size below 50 nm favor the CNT growth and those larger than 60 nm, favor the CNF growth. Both base and tip growth modes could be observed in direct growth; the first one due to strong adhesion of catalytic surface nano-features to the substrate, and the second one due to the surface break-up and dusting.

2- Growth of CNTs on SS with ferrocene external catalyst is highly influenced by the catalyst morphology and its interaction with the substrate. The fraction of CNFs is insignificant due to small average size of formed catalyst particles. These catalysts, formed by dissociation of ferrocene dissolved in toluene, deposit not only on the substrate surface, but also on the CNT walls and cause the growth of CNT offshoots. Due to likely strong adhesion of these iron based particles to SS substrate, tip growth mode is not activated in this method. Catalytic activity of the external catalyst seems stronger than that of the substrate nano-hills. This is inferred not only from the thicker and denser

carbon carpet formed in CG sample, but also from the dominance of characteristic features of catalyzed growth which have overshadowed the symptoms of probable contribution of direct growth mechanisms.

Acknowledgments

Authors acknowledge partial support from Fondazione Cariplo, Italy, through contract 2011-0336, “Nanomaterials for Blue Energy: renewable energy from capacitive mixing by using supercapacitors with nanostructured electrodes (NANOBLUE)”.

References

1. G. D. Nessim, *Nanoscale*, **2**, 1306 (2010).
2. V. Jourdain and C. Bichara, *Carbon*, **58**, 2–39 (2013).
3. W. Z. Li et al., *Science*, **274**, 1701–1703 (1996).
4. Z. F. Ren et al., *Science*, **282**, 1105–1107 (1998).
5. K. Gong et al., *Anal. Sci. Int. J. Jpn. Soc. Anal. Chem.*, **21**, 1383–1393 (2005).
6. Y. Oren, *Desalination*, **228**, 10–29 (2008).
7. A. G. Nasibulin et al., *Chem. Phys. Lett.*, **417**, 179–184 (2006).
8. T. Y. Lee et al., *Surf. Coatings Technol.*, **169–170**, 348–352 (2003).
9. M. A. Ermakova, D. Y. Ermakov, A. L. Chuvilin, and G. G. Kuvshinov, *J. Catal.*, **201**, 183–197 (2001).
10. P. Chen, H.-B. Zhang, G.-D. Lin, Q. Hong, and K. R. Tsai, *Carbon*, **35**, 1495–1501 (1997).
11. R. Kavian, A. Vicenzo, and M. Bestetti, *J. Mater. Sci.*, **46**, 1487–1493 (2011).
12. Y. Li et al., *J. Phys. Chem. B*, **105**, 11424–11431 (2001).
13. D. Venegoni et al., *Carbon*, **40**, 1799–1807 (2002).
14. Y. Li, J. Liu, Y. Wang, and Z. L. Wang, *Chem. Mater.*, **13**, 1008–1014 (2001).
15. B. D. Yao and N. Wang, *J. Phys. Chem. B*, **105**, 11395–11398 (2001).
16. J.-P. Kim et al., *Thin Solid Films*, **517**, 1136–1140 (2008).
17. Y.-R. Ma et al., *J. Magn. Magn. Mater.*, **282**, 61–64 (2004).
18. N. K. Reddy, J.-L. Meunier, and S. Coulombe, *Mater. Lett.*, **60**, 3761–3765 (2006).
19. Z. P. Huang et al., *Appl. Phys. Lett.*, **73**, 3845 –3847 (1998).
20. Q. Yang, Y. Tang, S. L. Yang, Y. S. Li, and A. Hirose, *Carbon*, **46**, 589–595 (2008).
21. L. Camilli et al., *Carbon*, **49**, 3307–3315 (2011).
22. C. E. Baddour et al., *Carbon*, **47**, 313–318 (2009).
23. C. E. Baddour and J. Meunier, in *8th IEEE Conference on Nanotechnology, 2008. NANO ’08,*, p. 752–755 (2008).
24. C. E. Baddour, D. C. Upham, and J.-L. Meunier, *Carbon*, **48**, 2652–2656 (2010).
25. X. H. Nguyen, Y. B. Lee, C. H. Lee, and D.-S. Lim, *Carbon*, **48**, 2910–2916 (2010).
26. N. Sabeti Nejad, M. M. Larijani, M. Ghoranneviss, P. Balashabadi, and A. Shokouhy, *Surf. Coatings Technol.*, **203**, 2510–2513 (2009).
27. N. Sano, Y. Hori, S. Yamamoto, and H. Tamon, *Carbon*, **50**, 115–122 (2012).
28. R. L. Vander Wal and L. J. Hall, *Carbon*, **41**, 659–672 (2003).
29. V. Martínez-Hansen et al., *Catal. Today*, **147**, S71–S75 (2009).

30. M. Karwa, Z. Iqbal, and S. Mitra, *Carbon*, **44**, 1235–1242 (2006).
31. Y.-K. Ko, W.-B. Lee, C.-W. Lee, and S. Yoo, *Mater. Res. Bull.*, **45**, 343–347 (2010).
32. I. Kunadian, R. Andrews, D. Qian, and M. Pinar Mengüç, *Carbon*, **47**, 384–395 (2009).
33. M. Delmas et al., *Nanotechnology*, **23**, N.105604: 1–8 (2012).
34. Kanchan M. Samant, Santosh K. Haram, and Sudhir Kapoor, *Pramana - J. Phys.*, **68**, 51–60 (2007).
35. Z. Wang, Q. Wu, F.-Y. Zhang, and Y.-Y. Cui, *Mater. Lett.*, **61**, 1955–1958 (2007).
36. M. Hashempour, A. Vicenzo, F. Zhao, and M. Bestetti, *Carbon* (2013), *http://dx.doi.org/10.1016/j.carbon.2013.06.087*.
37. D. Park, Y. H. Kim, and J. K. Lee, *J. Mater. Sci.*, **38**, 4933–4939 (2003).
38. P. Szakálos, thesis, Kungl. Tekniska högskolan (KTH), Institutionen för materialvetenskap, Stockholm (2004).
39. P. Szakálos, R. Pettersson, and S. Hertzman, *Corros. Sci.*, **44**, 2253–2270 (2002).
40. K. J. Stevens et al., *Mater. Sci. Eng.*, **385**, 292–299 (2004).
41. S. Esconjauregui, C. M. Whelan, and K. Maex, *Carbon*, **47**, 659–669 (2009).
42. A. K. Schaper, H. Hou, A. Greiner, and F. Phillipp, *J. Catal.*, **222**, 250–254 (2004).
43. H. Yoshida, S. Takeda, T. Uchiyama, H. Kohno, and Y. Homma, *Nano Lett.*, **8**, 2082–2086 (2008).
44. X. Chen, R. Wang, J. Xu, and D. Yu, *Micron*, **35**, 455–460 (2004).
45. Z. . Pan et al., *Chem. Phys. Lett.*, **299**, 97–102 (1999).
46. C. Ducati, I. Alexandrou, M. Chhowalla, G. A. J. Amaratunga, and J. Robertson, *J. Appl. Phys.*, **92**, 3299–3303 (2002).
47. E. Pippel, J. Woltersdorf, and R. Schneider, *Mater. Corros.*, **49**, 309–316 (1998).
48. E. Pippel, J. Woltersdorf, H. J. Grabke, and S. Strauss, *Steel Res.*, **66**, 217–221 (1995).
49. N. Koprinarov, M. Konstantinova, and M. Marinov, *Solid State Phenom.*, **159**, 105–108 (2010).